Validation of advanced material models using the crossdie test

H. H. Wisselink [*] ***, M. S. Niazi*** [*] ***and J. Huétink*** [**]

[*]*Materials Innovation Institute*
P.O. Box 5008, 2600GA Delft, The Netherlands
[**]*Faculty of Engineering Technology, University of Twente*
P.O. Box 217, 7500AE Enschede, The Netherlands
h.wisselink@m2i.nl, m.niazi@m2i.nl, j.huetink@utwente.nl

Abstract: The crossdie test, i.e. deepdrawing with cross shaped tools, is used in industry to asses the formability of the sheet material. The strain path of the material in this test is non-proportional. The effect of strain path changes can be modelled with the Teodosiu & Hu model. Therefore this model is applied to describe the Bauschinger and cross hardening effects present in the crossdie test to improve the simulation results. Less ductile materials, such as high strength steels or aluminium, show already ductile damage before necking. Therefore damage should be included in the material models to predict failure accurately. An anisotropic continuum damage model is used to simulate the crossdie test. In this model damage is not a scalar but a second order tensor, which means that the softening has a different effect in different directions.

Results of simulations using both advanced material models and a simple material model will be compared with a set of experimental data. The predictions of forming processes can be improved further if both damage and strain path changes are included in the simulations.

Keywords: Strain path changes, Teodosiu&Hu, Anisotropic damage, crossdie test

1. INTRODUCTION

The crossdie test, i.e. deepdrawing with cross shaped tools, is used in industry to asses the formability of the sheet material. The crossdie value (CD-value) is the largest possible blank size, which can be used to create a product of certain depth without any sign of necking [**Atzema et al., 2004**]. An example of a cross die product is shown in Figure 1. This test does represent the actual sheet forming processes better than traditional deep drawing tests with round or square cups. However FEM simulations of the crossdie test using standard material models and standard friction conditions show remarkable differences with the measured data [**Roelofsen and ten Horn, 2005**]. Therefore it is investigated whether more advanced material models will improve this.

During the crossdie test the material is deformed in many different strain paths and also non-proportional strain paths are present as will be shown in Section 2.. The IF-steel DC06 shows a strong strain-path dependent material behavior. Therefore this material

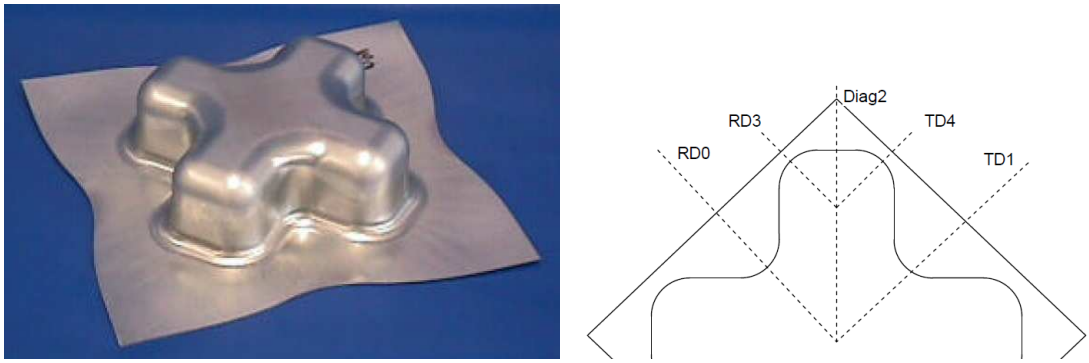

*Figure 1; Crossdie product, with sections indicated [***Atzema et al., 2004***].*

should be simulated with a material model, which is able to describe the Bauschinger and cross hardening effects present in the crossdie test, such as the Teodosiu & Hu model. This material model is described and applied to the crossdie test Section 3..

Less ductile materials, such as high strength steels or aluminium, show already ductile damage before necking. Therefore damage should be included in the material models to predict failure accurately. In Section 4. an anisotropic damage model is decribed and applied to predict the failure of the dual phase steel DP600 in the cross die test. Both described material models have been implemented in the implicit in house FEM code DIEKA [**DiekA development group, 2011**]. Results of simulations using both advanced material models and a simple material model will be compared with strains measured along the representative sections indicated in Figure 1.

The parameters for the cross-die test used in this paper are given in Table I. The blanksize is taken such that the product is about to fail. Although this test is used to characterise the material other effects as tool deformation and friction play an important role as well [**Lingbeek et al., 2008**, **Hol et al., 2010**]. However these effects are ignored and the tools are taken rigid and a constant Coulomb friction coefficient is used.

2. STRAIN PATH CHANGE INDICATOR

A strain path change indicator (SPCI) has been developed by [**van Riel and van den Boogaard, 2008**, **van Riel, 2009**], which indicates whether the strain path is proportional, orthogonal or reversed. This SPCI can be used for post-processing and is implemented in DIEKA. When a SPCI is applied to the results of a first simple and fast simulation of a metal forming process, it can be assessed quickly, whether simple and fast material models are sufficiently accurate or more complex and time consuming material models are needed. A quick selection ensures that costly models are only applied for the cases where strain path changes are expected to have a significant impact on the simulation results.

The strain path change indicator as proposed by [**van Riel, 2009**] does not compare

two sequential strain increments, but instead the strain history is compared with the current strain increment. This makes the indicator step size independent and continuous strain path changes are still detected for small increments. The evolution of the history of the strain path $\mathbf{G}$ is described by:

$$\dot{\mathbf{G}} = \dot{\boldsymbol{\varepsilon}} - c\dot{\varepsilon}^{p}_{eq}\mathbf{G} \tag{1}$$

The parameter c determines how much the history of the strain $\boldsymbol{\varepsilon}$ contributes to the evolution of $\mathbf{G}$. The strain path change indicator ξ is defined as:

$$\xi = \frac{\mathbf{G} : \dot{\boldsymbol{\varepsilon}}}{\|\mathbf{G}\| \, \|\dot{\boldsymbol{\varepsilon}}\|} \tag{2}$$

Differential Equation 1 can be solved, keeping $\dot{\boldsymbol{\varepsilon}}$ and $\dot{\varepsilon}^{p}_{eq}$ constant. The implementation for a time increment then reads:

$$\mathbf{e_1} = \mathbf{e_0} \exp[-c\Delta\varepsilon^{p}_{eq}] + \frac{\Delta\boldsymbol{\varepsilon}\left(1 - \exp[-c\Delta\varepsilon^{p}_{eq}]\right)}{c\Delta\varepsilon^{p}_{eq}} \tag{3}$$

$$\xi = \frac{\mathbf{e_1} : \Delta\boldsymbol{\varepsilon}}{\|\mathbf{e_1}\| \, \|\Delta\boldsymbol{\varepsilon}\|} \tag{4}$$

with $\mathbf{e_0}$ and $\mathbf{e_1}$ the values of the strain history at the begin and end of an increment and $\Delta\varepsilon^{p}_{eq}$ and $\Delta\boldsymbol{\varepsilon}$ the plastic strain increments. When the plastic strain increment is zero (unloading) the indicator is undefined and set to two ($\xi = 2$). In all other cases the indicator will have value in the range $\xi = [-1, 1]$. An indicator value of $\xi = 1$ indicates proportional loading, where $\xi = -1$ and $\xi = 0$ indicate reverse loading and orthogonal loading respectively. This strain path change indicator is demonstrated on the cross die in Figure 2 using a standard material model. It can be seen that the SPCI indicates a band where the strain path changes. The results on the lower and upper surface of the sheet are different Figure 2(a).

3. TEODOSIU & HU MODEL

Teodosiu and co-workers [**Teodosiu and Hu, 1995**, **Uenishi and Teodosiu, 2004**, **Haddadi et al., 2006**, **van Riel, 2009**] developed a material model which is able to describe the Bauschinger effect; the transient hardening and the work hardening stagnation after a load reversal, and also the characteristic overshoot in stress after an orthogonal strain path change. The main features of this model will be described here briefly. In essence it is a combined isotropic-kinematic hardening model where the parameters become functions of the strain history. The main components in this model are the 4th order strength of dislocation structure tensor $\mathbf{S}$ and the 2nd order Polarity tensor $\mathbf{P}$, which describe the influence of the micro-structure on the mechanical behaviour. The evolution equations for $\mathbf{S}$ and $\mathbf{P}$,which depend on the strain-rate direction, can be found in the references.

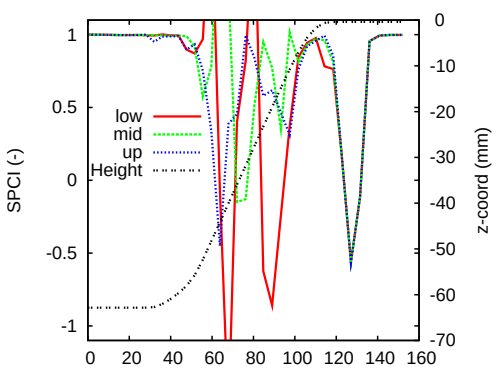

(a) ξ along section RD0

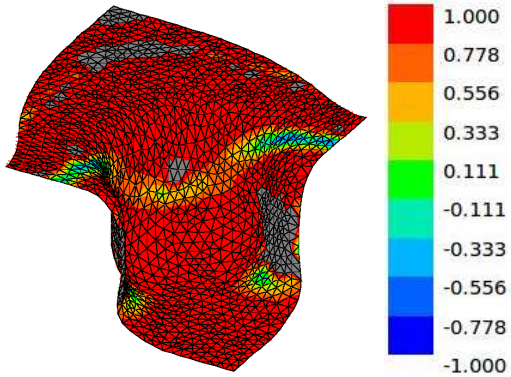

(b) ξ on the midplane

Figure 2; Calculated values of the Strain path Change Indicator (-1=reverse, 0=orthogonal, 1=proportional) for the crossdie ($c = 10$).

In the Teodosiu & Hu model, the classical yield function is employed.

$$\phi = \sigma_{eq}(\boldsymbol{\sigma} - \boldsymbol{\alpha}) - \sigma_f. \tag{5}$$

For the definition of the equivalent stress the Vegter model is used [**Vegter and van den Boogaard, 2006**]. The flow stress is written as:

$$\sigma_f = \sigma_{wh} + \sigma_{dyn} + m \left\| \mathbf{S} \right\| \tag{6}$$

Where σ_{wh} describes the isotropic hardening due to the cellular dislocation structure. Here the isothermal Bergström–Van Liempt hardening model is used [**Vegter et al., 2003**]:

$$\sigma_{wh} = \sigma_{f0} + d\sigma_m \left(\beta_v \left(\varepsilon + \varepsilon_0\right) + \left\{1 - \exp[-\omega(\varepsilon + \varepsilon_0)]\right\}^n\right) \tag{7}$$

The strain rate influence is incorporated similarly to [**Uenishi and Teodosiu, 2004**] and is given by the dynamic stress σ_{dyn}.

$$\sigma_{dyn} = \sigma_{v0} \left(1 + \frac{k\,T}{\Delta G_0} \ln\left(\frac{\dot{\varepsilon}}{\dot{\varepsilon}_0}\right)\right)^p \tag{8}$$

The last term in Equation 6 describes the isotropic hardening due the strength of the dislocation sheets. The influence of $\mathbf{S}$ is distributed across the isotropic and kinematic hardening via the material parameter m.

Kinematic hardening is employed via the effective stress in the calculation of the equivalent stress in Equation 5. The evolution of the back stress $\boldsymbol{\alpha}$ is modelled by an Armstrong–Frederick-like saturation law:

$$\dot{\boldsymbol{\alpha}} = C_\alpha \left(\alpha_s \mathbf{N} - \boldsymbol{\alpha}\right) \dot{\lambda} \tag{9}$$

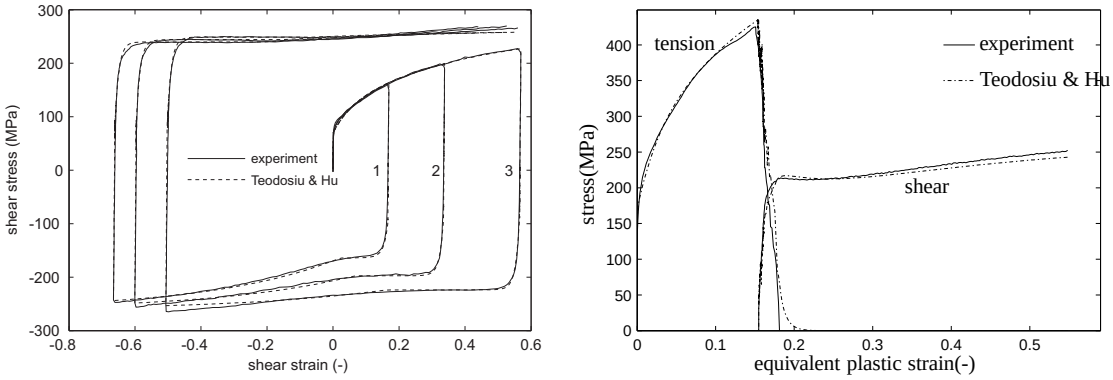

(a) Cyclic test (b) Continuous orthogonal test

Figure 3; The stress–strain curves for the experiments and the prediction of the Teodosiu & Hu model for DC06 material.

Table I; Process settings crossdie test.

material	DC06	DP600		DC06	DP600
Sheet thickness (mm)	0.7	1.0	Sheet size (mm)	285	270
Blankholder force (kN)	160	483	Depth setting (mm)	60	40
Punch speed (mm/s)	40	40	Friction coefficient (-)	0.13	0.06

where $\mathbf{N}$ is the normal to the yield surface, representing the strain rate direction and C_α defines the saturation rate. The saturation value of the back-stress is given by α_s, which is not a material parameter, but an internal variable depending on $\mathbf{S}$.

The number of material parameters which need to be determined for the Teodosiu & Hu model becomes large. Furthermore the number of material tests needed is increasing as well. [**van Riel, 2009**] has determined these parameters for a number of sheet materials using tensile tests, cyclic shear tests and orthogonal tests performed on the Twente biaxial Tester. It can be seen in Figure 3 that the Teodosiu & Hu model captures the work hardening stagnation that occurs after the load reversal in the cyclic tests and the overshoot in the orthogonal test. However the stress is underestimated at higher strains.

Simulations of the crossdie test are carried out with four material models for DC06 material all using the same Vegter yield locus, but different hardening models:

ISO: Nadai Isotropic hardening only using a Nadai relation [**van Riel, 2009**].
ISO: Bergstrom Isotropic hardening only using the Bergström relation of Equation 7 and Equation 8 [**Vegter et al., 2003**].
TEO: Voce The Teodosiu & Hu model using a Voce law for the isotropic hardening part (Equation 7 only with $\beta = 0$ and $n = 1$) [**van Riel, 2009**].
TEO: Voce + rate As the previous one but now also with strain-rate hardening (Equation 8).

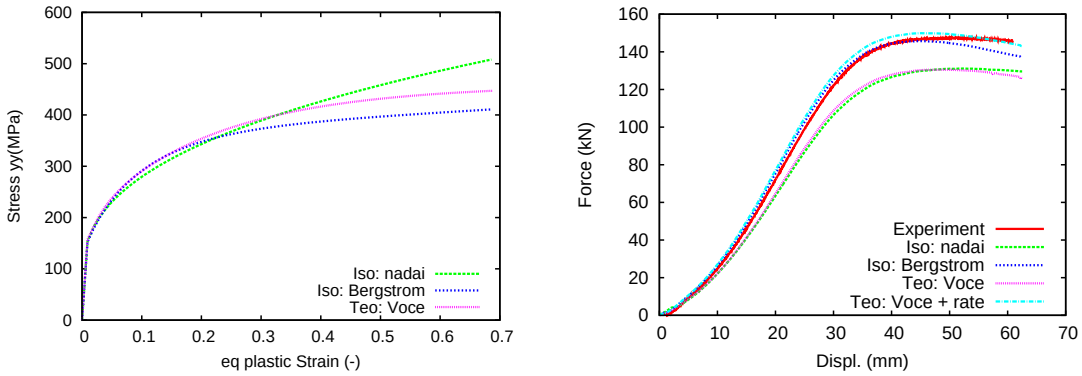

(a) uniaxial tension (b) Force-displacement

Figure 4; Results for DC06 material using an isotropic and the Teodosiu & Hu material model for uniaxial tension and the crossdie test.

First these models are compared for monotonic loading in a simulation of a quasi-static uniaxial tension test. It can be seen in Figure 4(a) that the response for large strains is different. The response for the cross-die test is presented in Figure 4(b). This figure shows that taking into account strain-rate hardening has more effect on the total punch force than the strain hardening mode as strain-rates go up to $1/s$ in this test,

The calculated strains in the critical section Diag2 are compared with the measured strains in Figure 5. All models predict the strains well. However at the critital point at an arc length of 100mm there are larger differences. Models without strain-rate hardening predict much more thinning than models with strain-rate hardening, which delays failure. Furthermore the hardening rate at large strains (Figure 4(a)) becomes important here.

4. ANISOTROPIC DAMAGE MODEL

The isotropic and anisotropic continuum damage models of [**Lemaitre and Desmorat, 2005**] are used to simulate the crossdie test. The isotropic damage model uses a scalar damage variable d. In the anisotropic model damage is not a scalar but a second order tensor $\mathbf{D}$. This means that the softening has a different effect in different directions and a load induced anisotropy can develop in initially isotropic material. The damage evolution law is given by a function of the plastic strain rate tensor/ equivalent plastic strain rate and triaxiality:

$$\dot{\mathbf{D}} = \left(\frac{\bar{Y}}{S}\right)^s \left|\dot{\boldsymbol{\varepsilon}}^p\right| \qquad \text{for} \qquad \varepsilon_1^p > \varepsilon_D^p \qquad \text{upto} \qquad D_1 > D_c \tag{10}$$

$$\dot{d} = \left(\frac{\bar{Y}}{S}\right)^s \dot{\varepsilon}_{eq}^p \qquad \text{for} \qquad \varepsilon_{eq}^p > (\varepsilon_{eq}^p)_D \qquad \text{upto} \qquad d > D_c \tag{11}$$

The damage starts growing when the major principal strain ε_1^p is larger than the

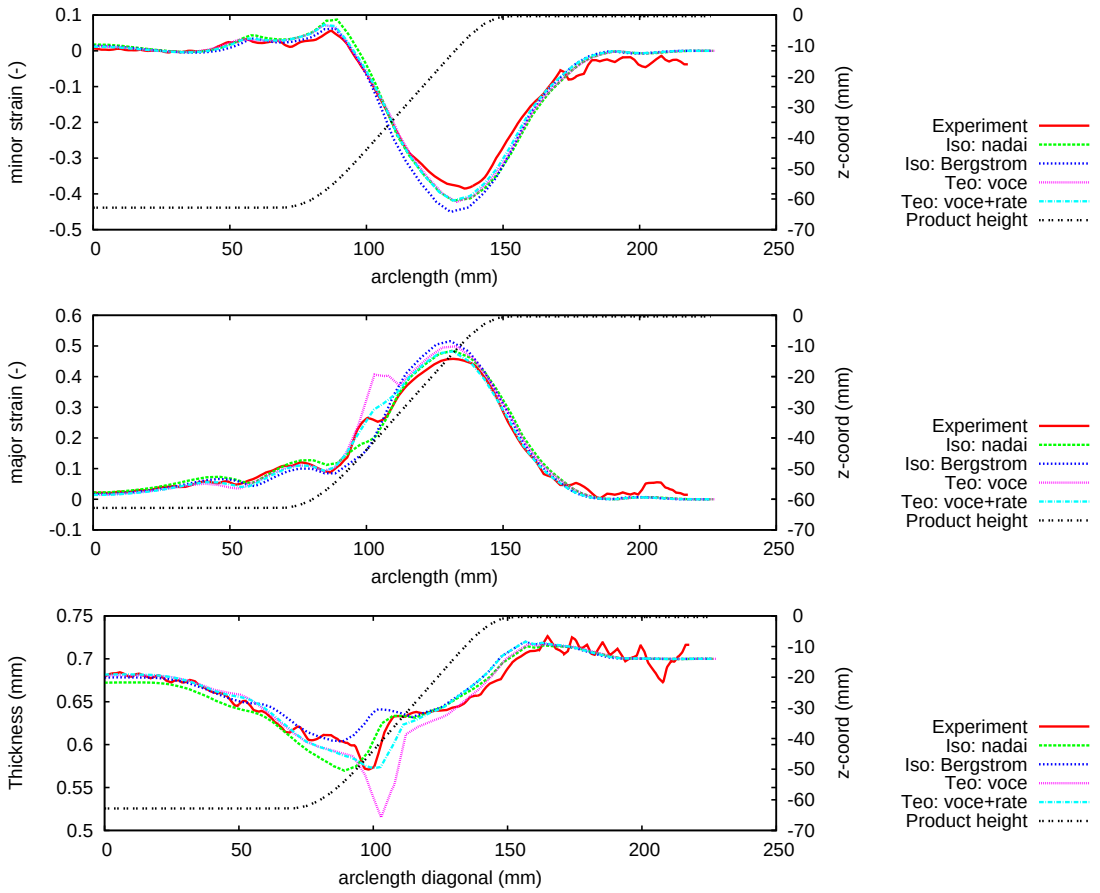

Figure 5; Strains along Diag2 measured from the center for the cross-die test for DC06 material using isotropic and Teodosiu & Hu material models.

threshold ε_D^p and keeps growing until the major principal damage D_1 is equal to the critical damage D_c. $\tilde{\boldsymbol{\sigma}}$ is the effective stress. with the energy release rate $\bar{Y}$ and the triaxiality factor $\bar{R}_v$:

$$\bar{Y} = \frac{\tilde{\sigma}_{eq}^2 \bar{R}_v}{2E} \qquad \bar{R}_v = \frac{2}{3}(1+\nu) + 3(1-2\nu)\left(\frac{\tilde{\sigma}^H}{\tilde{\sigma}_{eq}}\right)^2 \tag{12}$$

Some adaptations have been made to the original model of [**Lemaitre and Desmorat, 2005**]. Details can be found in [**Niazi et al., 2011**]. The damage evolution for negative triaxialities is decreased by selecting a large value for u_f to avoid failure under compression.

$$S = S \qquad \text{for} \qquad \tilde{\sigma}^H \geq 0 \qquad \text{and} \qquad S = u_f S \qquad \text{for} \qquad \tilde{\sigma}^H < 0 \tag{13}$$

and the parameters s and D_c are made a function of strain-rate, to slow down damage development and increase the critical damage for higher strain-rates.

$$s = s(\dot{\varepsilon}) \qquad \text{and} \qquad D_c = D_c(\dot{\varepsilon}) \tag{14}$$

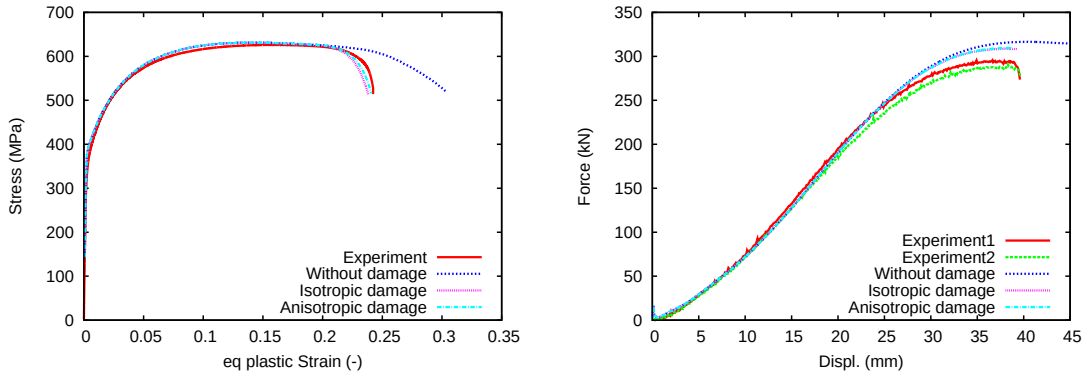

(a) Quasi-static tensile test (b) Cross die test

Figure 6; Validation of damage parameters of DP600 material.

The four damage parameters are identified for DP600 material using the fast identification procedure of [**Lemaitre and Desmorat, 2005**] using a quasi static tensile test and a low cycle fatigue test. The parameters for the isotropic and anisotropic material model are identical. A VonMises flowrule is used as the plastic behaviour of this material is almost isotropic. Again the Bergström-vanLiempt isotropic hardening law is used. Material Induced Anisotropy in damage (MIAD), which will make the parameters direction dependent, is not (yet) taken into account. The identified parameters are validated by simulations of the tensile test used to determine them, which show a good correlation (Figure 6(a)) and tensile tests at larger strain-rates. The damage models are applied to a crossdie test which fails around a punch displacement of 39.6mm. (Experiment1 localised, Experiment2 not yet). The simulations with the damage models predict failure around 39mm punch depth, where the strain-rate dependency of the damage parameters was needed.

The strains at the critical section of the product of Experiment2, are compared with the simulation results in Figure 7. The simulations with damage predict larger strains than the simulation without damage and the experiment, which did not localize yet. This is caused by the development of damage in this area which leads to localisation of the strains. The simulations with damage predict failure at the correct position as can be seen in Figure 8. An advantage of the anisotropic model is that the damage tensor stores additional information about the direction of the crack growth.

5. DISCUSSION

The predictions of forming processes can be improved further if both damage and the effect of strain path changes are included in the simulations. However till now both models can not be used together. It will be interesting to combine both models.

The presented advanced material models are essentially 3D models and should be

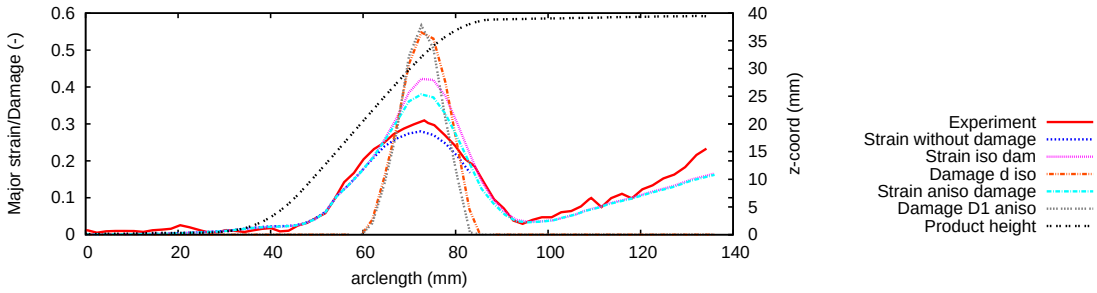

Figure 7; Strains along RD0 measured from the center for the cross-die test for DP600 material using isotropic and anisotropic damage material model.

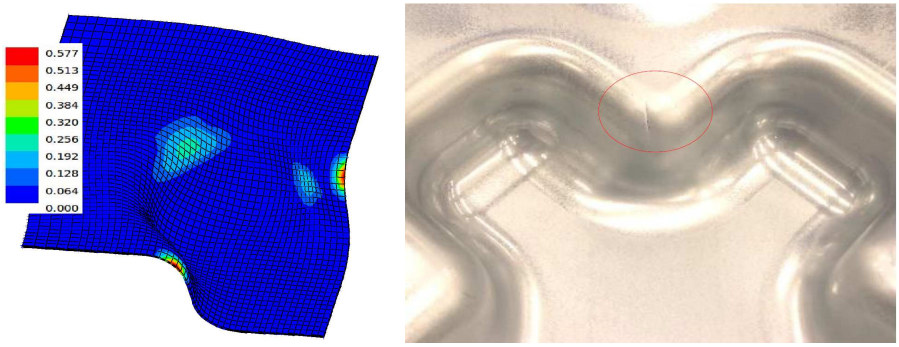

(a) Maximum principal Damage (b) Failed product

Figure 8; Comparison of location of failure for DP600 material.

used with solid elements. However using an extra iteration loop in the stress update shell elements can be used as well. In all cases these models need more calculation time than the standard material models. Multi-threading proved to be effective to reduce the calculation times of expensive material models. The presented SPCI gives a good indication whether strain-path dependent material have to be used.

The crossdie simulations of Section 3. show that when including the effect of strain path changes other aspects as large strains and strain-rate hardening should not be neglected, otherwise the results will not improve. A damage model has been applied to the crossdie test. The failure could be predicted succesfully by using parameters determined from a simple tensile test.

ACKNOWLEDGEMENTS

This research was carried out under the project numbers MC1.03158, MA.09170 and M61.1.08308 in the framework of the Program of the Materials innovation institute M2i (www.m2i.nl).

REFERENCES

[**Atzema et al., 2004]** Atzema, E., ten Horn, C., and Vegter, H. (2004). Influence on tooling layout on forming process analysis. In *ECCOMAS 2004*.

[**DiekA development group, 2011]** DiekA development group (2011). *DiekA users manual, release 10.0*. www.dieka.org.

[**Haddadi et al., 2006]** Haddadi, H., Bouvier, S., Banu, M., Maier, C., and Teodosiu, C. (2006). Towards an accurate description of the anisotropic behaviour of sheet metals under large plastic deformations: Modelling, numerical analysis and identification. *International Journal of Plasticity*, 22:2226–2271.

[**Hol et al., 2010]** Hol, J., Alfaro, M. C., de Rooij, M., and Meinders, V. (2010). Multi-scale friction modeling for sheet metal forming. In *Proceedings of the International Conference on Tribology in Manufacturing Processes, ICTMP 2010*, pages 573–582.

[**Lemaitre and Desmorat, 2005]** Lemaitre, J. and Desmorat, R. (2005). *Engineering Damage Mechanics*. Springer, Berlin.

[**Lingbeek et al., 2008]** Lingbeek, R., Meinders, T., and Rietman, A. (2008). Tool and blank interaction in the cross-die forming process. *Int. Journal of Material Forming*.

[**Niazi et al., 2011]** Niazi, M., Wisselink, H., Meinders, T., and Huétink, J. (2011). Failure predictions for DP steel cross-die test using anisotropic damage. *Int. J. Damage Mechanics*. submitted.

[**Roelofsen and ten Horn, 2005]** Roelofsen, M. and ten Horn, C. (2005). How well do virtual stampings compare to real parts? In *IDDRG 2005 International Conference*.

[**Teodosiu and Hu, 1995]** Teodosiu, C. and Hu, Z. (1995). Evolution of the intergranular microstructure at moderate and large strains: Modelling and computational significance. In Shen, S.-F. and Dawson, P. R., editors, *Simulation of Materials Processing: Theory, Methods and Applications*, pages 173–182, Rotterdam. Balkema.

[**Uenishi and Teodosiu, 2004]** Uenishi, A. and Teodosiu, C. (2004). Constitutive modelling of the high strain rate behaviour of interstitial-free steel. *International Journal of Plasticity*, 20:915–936.

[**van Riel, 2009]** van Riel, M. (2009). *Strain path dependency in sheet metal, Experiments and models*. PhD thesis, University of Twente. http://doc.utwente.nl/73561/.

[**van Riel and van den Boogaard, 2008]** van Riel, M. and van den Boogaard, A. (2008). A strain path change indicator for use in sheet metal forming processes. In *IDDRG 2008 International Conference*.

[**Vegter et al., 2003]** Vegter, H., ten Horn, C. H., An, Y., Atzema, E. H., Pijlman, H. H., van den Boogaard, T. H., and Huétink, H. (2003). Characterisation and modelling of the plastic material behaviour and its application in sheet metal forming simulation. In *VII International Conference on Computational Plasticity*.

[**Vegter and van den Boogaard, 2006]** Vegter, H. and van den Boogaard, A. (2006). A plane stress yield function for anisotropic sheet material by interpolation of biaxial stress states. *International journal of plasticity*, 22(3):557–580.